Tuning the Effective $\mathcal{PT}$ Phase of Plasmonic Eigenmodes

Alessandro Tuniz,[1,*] Torsten Wieduwilt,[2] and Markus A. Schmidt[2]
[1]Institute of Photonics and Optical Science (IPOS) and the University of Sydney Nano Institute (Sydney Nano), School of Physics, University of Sydney, NSW 2006, Australia
[2]Leibniz Institute of Photonic Technology (IPHT Jena), Albert-Einstein-Str. 9, 07745 Jena, Germany

(Received 10 July 2019; published 20 November 2019)

We experimentally observe an effective $\mathcal{PT}$-phase transition through the exceptional point in a hybrid plasmonic-dielectric waveguide system. Transmission experiments reveal fundamental changes in the underlying eigenmode interactions as the environmental refractive index is tuned, which can be unambiguously attributed to a crossing through the plasmonic exceptional point. These results extend the design opportunities for tunable non-Hermitian physics to plasmonic systems.

DOI: 10.1103/PhysRevLett.123.213903

Hermitian systems and their operators are used to describe a wide range of physical phenomena to predict the evolution of eigenstates via unitary operations containing purely real eigenvalues [1,2]. Recently, increasing attention has been dedicated to non-Hermitian systems, which are nonconservative and generally yield complex eigenvalue spectra [3]. Non-Hermitian systems are typically created by opening a Hermitian system to the environment by including dissipation and/or gain. Interestingly, coupled non-Hermitian systems can yield purely real eigenvalues, which respect parity-time ($\mathcal{PT}$) symmetry via an appropriate balance of gain and loss [4,5]. In an unbalanced scenario, a $\mathcal{PT}$-broken system shows complex conjugate eigenvalue pairs. The $\mathcal{PT}$-symmetric (PTS) and $\mathcal{PT}$-broken (PTB) regimes are separated by the exceptional point (EP), where the eigenvalues coalesce, which is associated with several interesting physical phenomena, such as level repulsion [6], reflectionless propagation [7], and topological phase transitions [8].

Photonics has been identified as the ideal landscape for investigating the subtle properties of non-Hermitian systems [5,9–11], since tailored amounts of optical gain and loss can be introduced by appropriately engineered materials and structures. Many important technological advances have recently been provided by EP photonics, such as sensitive modal manipulation [12], topological energy transfer [13], unidirectional propagation [14], and polarization conversion [15]. These advances rely on the unique characteristics of the eigenstates close to the EP—for example, even nanoscale events can be detected by measuring their impact on macroscopic eigenstates [16].

For many applications, balancing gain and loss is not necessary for accessing the underlying physics. Most investigations [5,7,17,18] harness *effective* $\mathcal{PT}$-symmetric systems with a global loss offset, where PTS and PTB states, separated by an EP, are achieved with eigenvalues that are shifted along the imaginary axis with respect to the perfectly balanced case. Such effective $\mathcal{PT}$-symmetric structures open up many opportunities in the design of photonic systems that harness $\mathcal{PT}$ symmetries without requiring gain, simplifying designs.

One state that can be used for non-Hermitian photonics is the surface plasmon polariton (SPP) [19], which is a propagating surface wave at a metal-dielectric interface. SPPs continue to attract attention due to their ability to confine light down to a fraction of the wavelength, and their high sensitivity to RI changes of the environment [19,20]. Owing to their large wave vectors, coupling energy to SPPs is often challenging. One approach relies on using (lossless) dielectric waveguides running parallel to (lossy) plasmonic waveguides [21], leading to systems with hybrid eigenmodes (EMs) and complex eigenvalues. Such dielectric-plasmonic systems are inherently non-Hermitian, and can be designed to possess an effective-$\mathcal{PT}$ phase transition—full $\mathcal{PT}$-symmetric properties can be recovered by re-introducing gain [22,23]. Despite its great potential in a multitude of areas [10], and a growing number of studies [22–26] including a recent report on nanostructures with localized plasmon resonances that show discrete frequency spectra [27], to the best of our knowledge effective $\mathcal{PT}$-phase transitions, tuned across the EP, have yet to be experimentally reported in plasmonic waveguides. Here, we experimentally observe the effective $\mathcal{PT}$-phase transition across the plasmonic EP of a tunable hybrid dielectric-plasmonic waveguide system. Transmission experiments reveal fundamental changes in the properties of the underlying system by tailoring the refractive index of the surrounding environment and unambiguously showing a crossing through the plasmonic EP.

The main features of such a system can be understood on the basis of mode hybridization using coupled mode theory (CMT). We consider the specific case of a lossless waveguide 1 (WG1) and lossy WG2, supporting modes with respective propagation constants $\beta_1 = \beta_1^R$ and $\beta_2 = \beta_2^R + i\beta_2^I$,

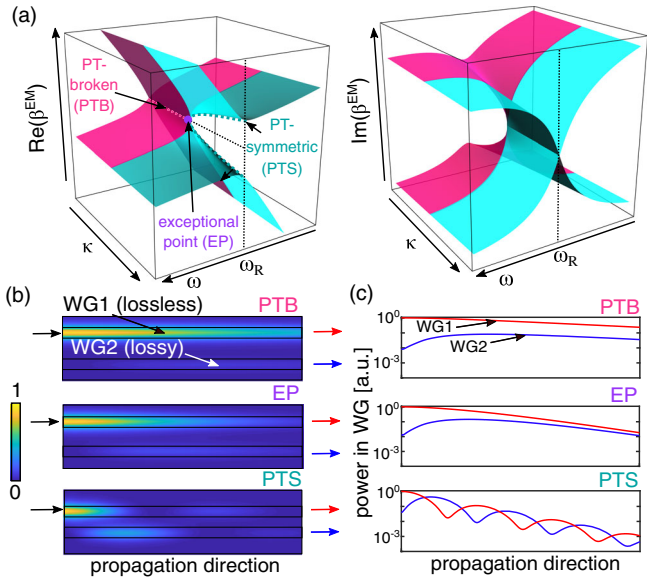

FIG. 1. (a) Real and imaginary part of β_j^{EM} calculated with the CMT model. (b) Example FEM calculations of the coupling behavior between a lossless and lossy WG at the phase matching point, highlighting the PTB and PTS regimes separated by the EP (black arrow: WG1 input; red and blue arrows: WG1 and WG2 output, respectively). (c) Axial power distribution in each waveguide, in the three regimes considered in (b). See Supplemental Material for further details [28].

and coupling constant κ, which for this particular case is assumed to be real [10]. The coupled mode equations can be written as

$$\frac{d}{dz}\begin{pmatrix} a_1 \\ a_2 \end{pmatrix} = -i\begin{pmatrix} \beta_1^R & \kappa \\ \kappa & \beta_2^R + i\beta_2^I \end{pmatrix}\begin{pmatrix} a_1 \\ a_2 \end{pmatrix}, \qquad (1)$$

where $a_{1,2}$ are the modal field amplitudes in each waveguide. Solutions of the form $a_j = A_j \exp(i\beta_j^{\mathrm{EM}} z)$ lead to hybrid EMs with propagation constants

$$\beta_j^{\mathrm{EM}} = \overline{\beta_R} + i\frac{\beta_2^I}{2} \pm \sqrt{\kappa^2 + \left(\Delta\beta_R + i\frac{\beta_2^I}{2}\right)^2}, \qquad (2)$$

where $\overline{\beta_R} = (\beta_1^R + \beta_2^R)/2$, $\Delta\beta_R = (\beta_1^R - \beta_2^R)/2$ is the dephasing, and $j = 1, 2$. We find that the CMT model [Fig. 1(a)] is in excellent agreement with simulations of a lossy 1D multilayer system [21] (see Supplemental Material for further details of the parameters used [28]). The model predicts different transmission characteristics near the EP, which occurs when the eigenvalues coalesce at a certain frequency ω_R such that $\sqrt{\kappa^2 + (\Delta\beta_R + i\beta_2^I/2)^2} = 0$, so that $\Delta\beta_R = 0$ (i.e., the phase-matching condition) and $\kappa = \beta_2^I/2$. Figures 1(b)–1(c) show finite element (FE) calculations that highlight the transmission characteristics close to the EP: the PTS regime is characterized by a periodic exchange of energy between the waveguides due to modal beating between EMs with different propagation constants—analagously to what occurs in Hermitian systems. The PTB regime is unique to non-Hermitian systems and presents no periodic energy exchange between waveguides at ω_R, since the real parts of the coupled eigenmodes are equal, resulting in an infinite beat length. These different regimes can be accessed at ω_R by changing κ/β_2^I.

To experimentally reveal the phase transition between PTB and PTS regimes across the EP, we consider a dielectric-plasmonic hybrid waveguide system with properties that can be tailored via the environmental refractive index (RI) [Fig. 2(a)]. The system is formed by a cylindrical SiO_2 waveguide (diameter: $d = 20\ \mu$m) coated with a gold nanofilm on one side (thickness: 30 nm). The EM dispersions are tuned by immersing the waveguide in liquids with different RI, with the interaction length determined by the length of the liquid column ℓ [20]. The uncoupled modes satisfy the phase matching condition at a wavelength λ_R only when the outer RI has a specific value—a scheme which has frequently been used for plasmonic sensing [19,20]. Here, we use commercially available analytes, identified by the refractive index n_{ID} at $\lambda = 589$ nm (see Supplemental Material [28] for the measured analyte and gold RI dispersions n_o).

We now consider the eigenstates of this system when changing the RI environment, and how this impacts coupling. Since $d \gg \lambda$, a qualitative understanding of the modal behaviour can be obtained using a 1D multilayer system that includes the RI distribution along the connection line between the center of the silica core and the azimuthal location of maximum gold film thickness [20]. The evolution of the eigenstate dispersions for this hybrid system [Fig. 2(b), where $n_{\mathrm{eff},j} = \beta_j^{\mathrm{EM}}/k_0$, $k_0 = 2\pi/\lambda$] show a clear transition from the PTB to PTS regimes. The EP is predicted close to $n_{\mathrm{ID}} = 1.42$, while its exact location will be highly sensitive to environmental conditions [16]. Note that the detailed properties of hybrid multimode dielectric-plasmonic waveguides are more complex than what the CMT model predicts, also because SPP modes are close to cutoff, with obvious implications on modal dispersion.

Calculations show that the transition across the plasmonic EP can be inferred from the transmission properties of this waveguide system by using different ℓ and RI environments. To illustrate this, we calculate the axial intensity distribution [Fig. 2(c)], and retrieve the transmitted power [Fig. 2(d)] using the modal evolution and interference of the two hybrid EMs excited by the fundamental mode of the corresponding dielectric waveguide [21]. The complex modal amplitudes at input and output are determined by overlap integrals between the fields at ℓ and the fundamental mode of the dielectric waveguide, allowing us to calculate the transmission through the hybrid system. The plots in Fig. 2(c) are calculated at λ_R, which in the PTB or PTS regime occurs, respectively, where the

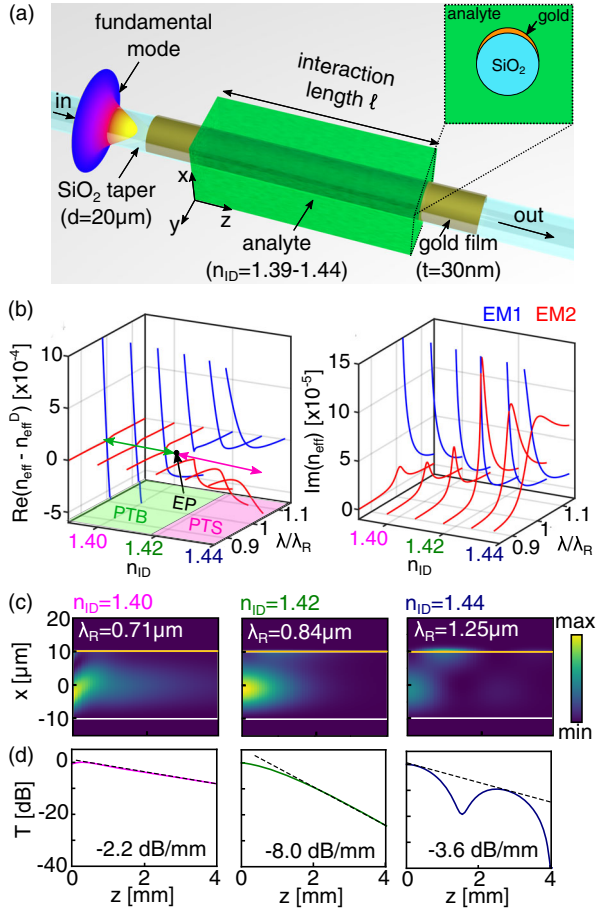

FIG. 2. (a) Schematic of the tunable plasmonic-dielectric waveguide system considered. A cylindrical SiO_2 waveguide, coated by a gold nanofilm, is immersed in a liquid with predefined RI. (b) Spectral distribution of $\mathrm{Re}(n_{\mathrm{eff},j} - n_{\mathrm{eff}}^{D})$ ($j = 1, 2$; n_{eff}^{D}: effective index of equivalent dielectric waveguide without gold film) and $\mathrm{Im}(n_{\mathrm{eff}})$ for EM1 and EM2 as a function of λ/λ_R (see Supplemental Material for λ_R values [28]). (c) Spatial distribution of the Poynting vector and (d) transmitted power into the dielectric waveguide at three example RIs. Dashed lines: fitted loss as labeled.

imaginary- or real- parts of n_{eff} cross (see Supplemental Material [28]). As expected, the PTS regime ($n_{\mathrm{ID}} = 1.440$) shows an oscillating damped energy distribution between the dielectric core and plasmonic layer [Fig. 2(c), right], due to modal beating of lossy EMs [Fig. 2(d), right]. In the PTB regime ($n_{\mathrm{ID}} = 1.400$), no such oscillations are observed [Fig. 2(c), left], and the transmitted power decays monotonically at smaller loss values [Fig. 2(d), left]. For $n_{\mathrm{ID}} = 1.420$ we find an intermediate case, where the transmission monotonically decays with the highest overall loss. Therefore, the two regimes can be distinguished by the axial power distribution, with the PTS case yielding an oscillatory behavior, while the PTB case shows a monotonic power decay, both of which have lower overall loss with respect to the loss at the EP (dashed lines). The fact that the EP possesses the highest overall loss in this kind of hybrid plasmonic system has been verified by a detailed numerical analysis (see Supplemental Material [28]). Since the loss of this system is maximum at the EP, the presence of a local loss maximum provides an additional property that can be used to confirm that an effective $\mathcal{PT}$-phase transition through the EP has occurred. Note that the simulations presented [Fig. 2(d)] enable a qualitative comparison to the experimental data and have been conducted in order to justify the choice of the hybrid waveguide used; the strong susceptibility on environmental influences, however, makes a quantitative comparison to experiments challenging.

We perform a comprehensive series of transmission experiments on the above system—details of sample preparation and experimental setup can be found in Ref. [21] and in the Supplemental Material [28]. Here,

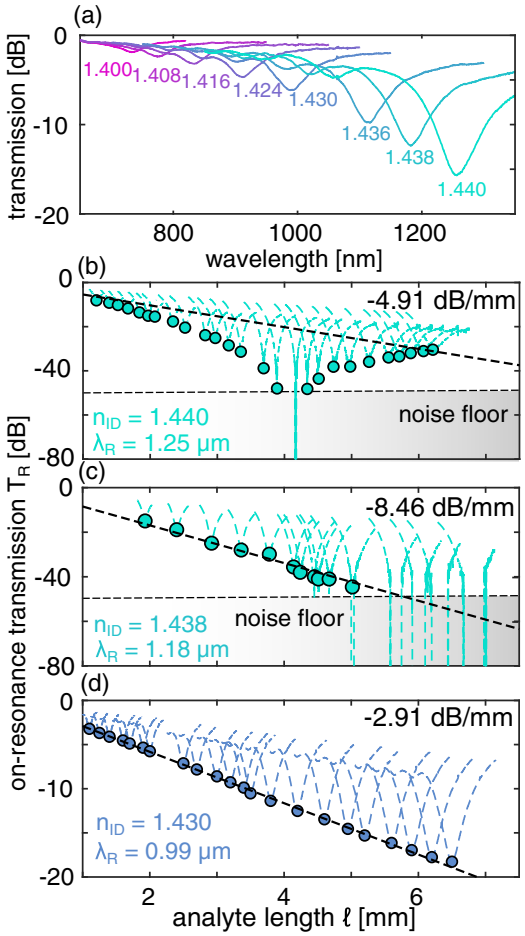

FIG. 3. (a) Measured spectral distribution of the power transmission through the hybrid waveguide (Fig. 2, $\ell = 1$ mm). Circles: measured on-resonance transmission as a function of ℓ for the analytes as labeled, showing the transition from (b) the PTS to (d) the PTB regime via (c) high-loss modes close to the EP. For each transmission dip, dashed lines show the full resonance spectrum centered in each transmission minimum (i.e., the horizontal axis of each spectrum is scaled by a factor ℓ/λ_R). Black dashed lines: fitted loss as labeled.

different interaction lengths were implemented using Teflon stubs of different length, which support defined droplets of analyte (spatial resolution: ± 0.05 mm). We first measured the spectral distribution of the transmission T for various analytes at constant interaction length [$\ell = 2$ mm, Fig. 3(a)]. We observe a transmission dip that shifts towards longer wavelengths and increases in contrast as n_{ID} is increased. The minimum transmission (T_R) for each n_{ID} occurs at resonant wavelengths λ_R. Calculations show that the transmission minimum is due to the interactions between the input mode and the excited hybrid EMs excited (see Supplemental Material [28]) and depends on both ℓ and the effective $\mathcal{PT}$-phase accessed. By analyzing λ_R as a function of RI at λ_R, we determined the experimental RI sensitivity given by $S = \partial\lambda_R/\partial n_o$, which exceeds 50 μm/RIU for $n_o > 1.43$ (see Supplemental Material [28]). This represents one of the highest values ever measured for any plasmonic device to date, and is due to operation near the cutoff [32] of the plasmonic mode.

Based on our previous analysis, we identify the transition between the two regimes by the different spatial power distribution (Fig. 2) by measuring the on-resonance power T_R vs ℓ at λ_R under three different conditions. A high analyte RI [$n_{\mathrm{ID}} = 1.440$, Fig. 3(b)] shows a strong dip in the spatial power transmission, indicating periodic energy exchange between the waveguides, i.e., directional coupling, confirming that this configuration is in the PTS regime. In contrast, a lower analyte RI [here $n_{\mathrm{ID}} \leq 1.438$, Figs. 3(c), 3(d)], yields an exponentially decreasing spatial power distribution with no dips, indicating no directional coupling, i.e., the PTB regime.

Note that due to power oscillations in the PTS case [Fig. 3(b)], it is difficult to estimate the overall loss; however, from the peak of the envelope we can estimate a lower bound of $\sim$4.91 dB/mm. This is higher than what is measured in the PTB regime [Fig. 3(d), 2.91 dB/mm], but lower than what is measured close to the EP [Fig. 3(c), 8.46 dB/mm], in qualitative agreement with the model [Figs. 2(b),(c)]—a further confirmation that the EP was crossed.

This study reveals that the effective $\mathcal{PT}$-symmetric and $\mathcal{PT}$-broken phases can be tuned through the EP in a non-Hermitian plasmonic system by adjusting the environmental refractive index. The proposed hybrid plasmonic system overcomes many of the challenges associated with observing exceptional points by making use of an additional degree of freedom [17,33]—in this case, the refractive index of the environment—to systematically control effective $\mathcal{PT}$ phases, which in practice allows us to lock the operation domain to the exceptional point. The PTB regime is particularly suitable for bioanalytic sensing, as the power transmission only weakly depends on propagation distance due to the moderate loss. This regime is suitable for addressing thin layers with large lateral dimensions (e.g., molecular layers or 2D materials), since the evanescent field homogeneously probes the material of interest along the entire waveguide, in contrast to all-dielectric systems. The PTS regime instead allows efficient and rapid energy transfer into plasmonic layers, leading to the extraordinary high RI sensitivity measured, which can be employed for highly demanding RI sensing applications, e.g., detecting single DNA-binding events or protein folding.

We have found that modes at the EP possess the highest overall loss for this particular system, a property which could be harnessed for plasmonic sensing applications near the EP. A recent theoretical report presented a similar result in a different context [34], warranting further study to verify its generality. Additionally, the phase indices of the EMs show a strong dependence of the effective mode index on the environmental RI, with additional implications for sensing. A modification of our structure could yield passive devices with extreme sensitivity at desired RIs (e.g., at the water index) to detect individual molecular events [35].

Our platform extends the capabilities of tunable non-Hermitian photonics near the EP [10]. The results and concepts presented here apply to any non-Hermitian waveguide, and immediately provide design tools for future EP-based photonic devices. Our system principally allows for restoring full $\mathcal{PT}$ symmetry by introducing a high gain material into the photonic waveguide [36,37]. Because of the unique properties of the two regimes and the unique dispersion characteristics near the EP, our study widens the scope of application areas of plasmonics, with applications in bioanalytics (e.g., sensing with exceptionally high sensitivity [16,38]), nonlinear frequency conversion (unique dispersion management [39]), signal processing (e.g., optical switching [40]), as well as quantum technologies [41], and topological physics [42].

A. T. acknowledges support from the University of Sydney Postdoctoral Fellowship scheme.

*alessandro.tuniz@sydney.edu.au

[1] N. Dunford and J. T. Schwartz, *Linear Operators. Parts 1 and 2* (Interscience, New York, 1957).
[2] R. Shankar, *Principles of Quantum Mechanics* (Springer Science & Business Media, New York, 2012).
[3] W. Heiss, J. Phys. A **45**, 444016 (2012).
[4] C. M. Bender and S. Boettcher, Phys. Rev. Lett. **80**, 5243 (1998).
[5] L. Feng, R. El-Ganainy, and L. Ge, Nat. Photonics **11**, 752 (2017).
[6] W. Heiss, Phys. Rev. E **61**, 929 (2000).
[7] L. Feng, Y.-L. Xu, W. S. Fegadolli, M.-H. Lu, J. E. Oliveira, V. R. Almeida, Y.-F. Chen, and A. Scherer, Nat. Mater. **12**, 108 (2013).
[8] M. S. Rudner and L. S. Levitov, Phys. Rev. Lett. **102**, 065703 (2009).
[9] R. El-Ganainy, K. G. Makris, M. Khajavikhan, Z. H. Musslimani, S. Rotter, and D. N. Christodoulides, Nat. Phys. **14**, 11 (2018).

[10] M.-A. Miri and A. Alù, Science **363**, eaar7709 (2019).
[11] Ş. Özdemir, S. Rotter, F. Nori, and L. Yang, Nat. Mater. **18**, 783 (2019).
[12] H. Hodaei, M.-A. Miri, M. Heinrich, D. N. Christodoulides, and M. Khajavikhan, Science **346**, 975 (2014).
[13] H. Xu, D. Mason, L. Jiang, and J. Harris, Nature (London) **537**, 80 (2016).
[14] Z. Wang, Y. Chong, J. D. Joannopoulos, and M. Soljačić, Nature (London) **461**, 772 (2009).
[15] A. U. Hassan, B. Zhen, M. Soljačić, M. Khajavikhan, and D. N. Christodoulides, Phys. Rev. Lett. **118**, 093002 (2017).
[16] W. Chen, Ş. K. Özdemir, G. Zhao, J. Wiersig, and L. Yang, Nature (London) **548**, 192 (2017).
[17] A. Guo, G. J. Salamo, D. Duchesne, R. Morandotti, M. Volatier-Ravat, V. Aimez, G. A. Siviloglou, and D. N. Christodoulides, Phys. Rev. Lett. **103**, 093902 (2009).
[18] B. Zhen, C. W. Hsu, Y. Igarashi, L. Lu, I. Kaminer, A. Pick, S.-L. Chua, J. D. Joannopoulos, and M. Soljačić, Nature (London) **525**, 354 (2015).
[19] L. Novotny and B. Hecht, *Principles of Nano-Optics* (Cambridge University Press, Cambridge, England, 2012).
[20] T. Wieduwilt, A. Tuniz, S. Linzen, S. Goerke, J. Dellith, U. Hübner, and M. A. Schmidt, Sci. Rep. **5**, 17060 (2015).
[21] A. Tuniz and M. A. Schmidt, Opt. Express **24**, 7507 (2016).
[22] H. Alaeian and J. A. Dionne, Phys. Rev. B **89**, 075136 (2014).
[23] J. R. Salgueiro and Y. S. Kivshar, IEEE J. Sel. Top. Quantum Electron. **22**, 60 (2016).
[24] A. Kodigala, T. Lepetit, and B. Kanté, Phys. Rev. B **94**, 201103(R) (2016).
[25] E. G. Turitsyna, I. V. Shadrivov, and Y. S. Kivshar, Phys. Rev. A **96**, 033824 (2017).
[26] H. Lourenço-Martins, P. Das, L. H. Tizei, R. Weil, and M. Kociak, Nat. Phys. **14**, 360 (2018).
[27] J.-H. Park, A. Ndao, W. Cai, L.-Y. Hsu, A. Kodigala, T. Lepetit, Y.-H. Lo, and B. Kanté, arXiv:1904.01073.
[28] See Supplemental Material at http://link.aps.org/supplemental/10.1103/PhysRevLett.123.213903 for further details of the coupled mode theory, a comparison between theoretical models and realistic waveguides, calculations to support the characteristics of the $\mathcal{PT}$-phase transition across the plasmonic exceptional point, and additional supporting figures, which includes Refs. [29–31].
[29] A. Yariv and P. Yeh, *Photonics: Optical Electronics in Modern Communications* (Oxford University Press, New York, 2006).
[30] Y.-F. Li and J. W. Y. Lit, J. Opt. Soc. Am. A **4**, 671 (1987).
[31] I. H. Malitson, J. Opt. Soc. Am. **55**, 1205 (1965).
[32] D. K. C. Wu, B. T. Kuhlmey, and B. J. Eggleton, Opt. Lett. **34**, 322 (2009).
[33] C. Shi, M. Dubois, Y. Chen, L. Cheng, H. Ramezani, Y. Wang, and X. Zhang, Nat. Commun. **7**, 11110 (2016).
[34] S. Ke, J. Liu, Q. Liu, D. Zhao, and W. Liu, Opt. Quantum Electron. **50**, 318 (2018).
[35] M. Chemnitz, G. Schmidl, A. Schwuchow, M. Zeisberger, U. Hübner, K. Weber, and M. A. Schmidt, Opt. Lett. **41**, 5377 (2016).
[36] D. Geskus, S. Aravazhi, S. M. García-Blanco, and M. Pollnau, Adv. Mater. **24**, OP19 (2012).
[37] Y.-S. Yong, S. Aravazhi, S. A. Vázquez-Córdova, J. L. Herek, S. M. García-Blanco, and M. Pollnau, J. Opt. Soc. Am. B **35**, 2176 (2018).
[38] Y. J. Zhang, H. Kwon, M.-A. Miri, E. Kallos, H. Cano-Garcia, M. S. Tong, and A. Alu, Phys. Rev. Applied **11**, 044049 (2019).
[39] M. Wimmer, A. Regensburger, M.-A. Miri, C. Bersch, D. N. Christodoulides, and U. Peschel, Nat. Commun. **6**, 7782 (2015).
[40] A. Lupu, H. Benisty, and A. Degiron, Opt. Express **21**, 21651 (2013).
[41] F. Quijandria, U. Naether, S. K. Özdemir, F. Nori, and D. Zueco, Phys. Rev. A **97**, 053846 (2018).
[42] Q. Zhong, M. Khajavikhan, D. N. Christodoulides, and R. El-Ganainy, Nat. Commun. **9**, 4808 (2018).